"Generation of Milled Surfaces Including Tool Dunamic and Wear" , ASME J. Eng. For Industry , Vol . 116, pp. 435-436, 1992.

[14] E. M. Lim , H. Y. Feng, C. H. Menq and Z. H. Lin,"The Prediction of Dimensional Error for Sculptured Surface Productions Using the Ball-end Milling Process , Part 1: Chip Geometry Analysis and Cutting Force Prediction", Int . J. Mach. Tools Manufact., Vol. 35, No. 8, pp. 1149-1169. 1995.

[15] H. Budak, Y. Altintas and E. J. Armarego, "Prediction of Milling of Force Coefficient from Orthogonal Cutting Data", J. of Manufacturing Science and Engineering , Vol. 118, pp. May 1996.

[16] M. C. Shaw, Metal Cutting Principles, Clarendon press, Oxford, 1984.

$\psi(\Theta, z)$	angle of a point on the cutting edge in global coordinates
k	angle in a vertical plane between a point on the cutting edge and z axis
τ	shear stress on shear plane
ϕ	shear angle
β	friction angle
β_n	normal friction angle
α_n	normal rake angle
α_e	effective rake angle
γ_0	tool clearance angle
Z	number of teeth
n	spindle speed
V	the cutting speed
dv	the volume of work material displaced by the tool penetration
Z_L	lower engagement of the cutting edge in z direction
Z_u	upper engagement of the cutting edge in z direction
Φ	angle of the planar surface relative to x direction
Ψ	angle of the planar surface relative to y direction
m_x	mass of tool system in x direction
m_y	mass of tool system in y direction
C_x	damping coefficient of tool system in x direction
C_y	damping coefficient of tool system in y direction
ξ_x	damping ratio in x direction
ξ_y	damping ratio in y direction
k_x	stiffness constant of tool system in x direction
k_y	stiffness constant of tool system in y direction
Δt	time step

References

[1] J. Tlusty and MacNeil , "Dynamics of cutting Forces in End Milling´´, Annals of CIRP, Vol. 24/ 1 , pp. 21-25 , 1975 .

[2] J. Tlusty and F. Ismail , ´´Basic Non - Linearity in Machining Chatter" , Annals of CIRP, Vol. 30, No . 1, pp. 299-304 , 1981

[3] J. Tlusty and F. Ismail , ´´Special Aspects of Chatter in Milling ´´ , ASME Journal of Vibration , Stress and Reliability in Design , Vol. 105 , pp. 24 32 , 1983.

[4] D. Montgomery and Y. Altintas , ''Mechanism of Cutting Force and Surface Generation in Dynamic Milling '' , ASME J. Eng. for Industry , Vol. 113, pp. 160-168, 1991.

[5] M. A. Elbestawi , F . Ismail , R. Du and B. C. Ullagaddi , ''Modeling Machining Dynamics Including Damping in The Tool - workpiece Interface" , ASME J. Eng . for Industry , Vol. 116, pp. 435-436, 1992.

[6] Y. Altintas and P. K. Chan , "In-process Detection and Suppression of Chatter in Milling" , Int . J. Mach . Tools Manufact ., Vol . 32, No . 3, pp. 329-347, 1992.

[7] M. Weck, Y. Altintas and C. Beer , "CAD Assisted Chatter - free NC Tool Path Generation in Milling" , Int . J. Mach . Tools Manufact ., Vol . 34, No .6, pp. 879-891, 1994.

[8] F. Abrari, M. A. Elbestawi and A. D. Spence, "On the Dynamics of Ball-end Milling Modeling of Cutting Forces and Stability Analysis" , Int . j.of Mach . Tools Manufact., Vol . 38, No. 3, pp. 215-237, 1998.

[9] Y. Altintas and P. Lee, "Mechanics and Dynamics of Ball End Milling", ASME J . Manufact . Science and End ., Vol . 120, pp. 684-691, 1998.

[10] M. Yang and H. Park , "The Prediction of Cutting Force in Ball-end Milling" , Int . J. Mach . Tools Manufact ., Vol. 31, No. 1, pp. 45-54, 1991.

[11] ACIS Geometric Modeler Application Guide, Special Technology Inc., Colorado, USA, 1975.

[12] D. W. Wu, "A New Approach of Formulating the Transfer Function for Dynamic Cutting processes" , ASME J. of Eng . for Industry , Vol 111, pp. 37-47, 1989.

[13] F. Ismail, M. A. Elbestawi, R. Du and K. Urbasik,

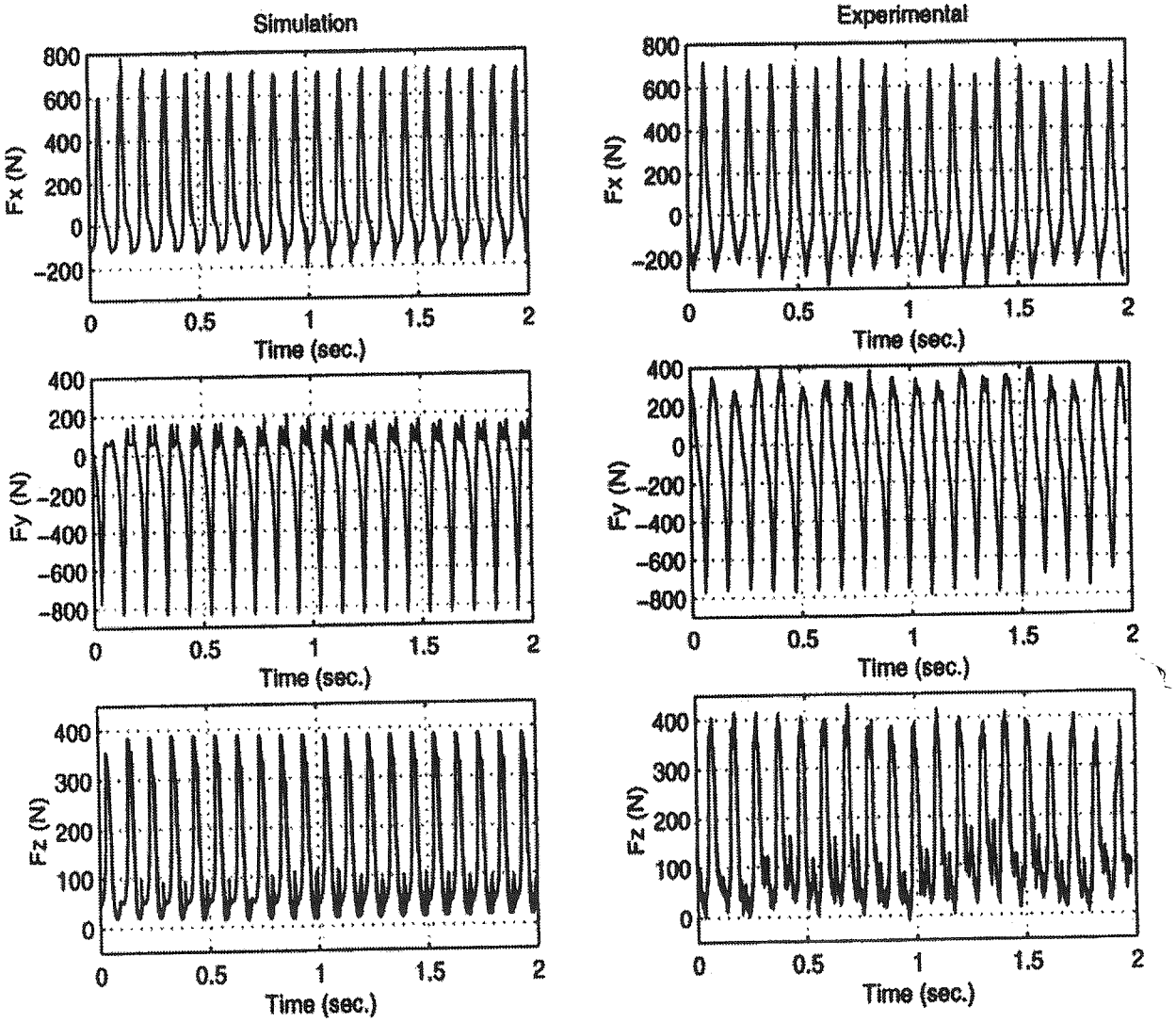

(b) Simulation of tool tip deflection in x and y directions

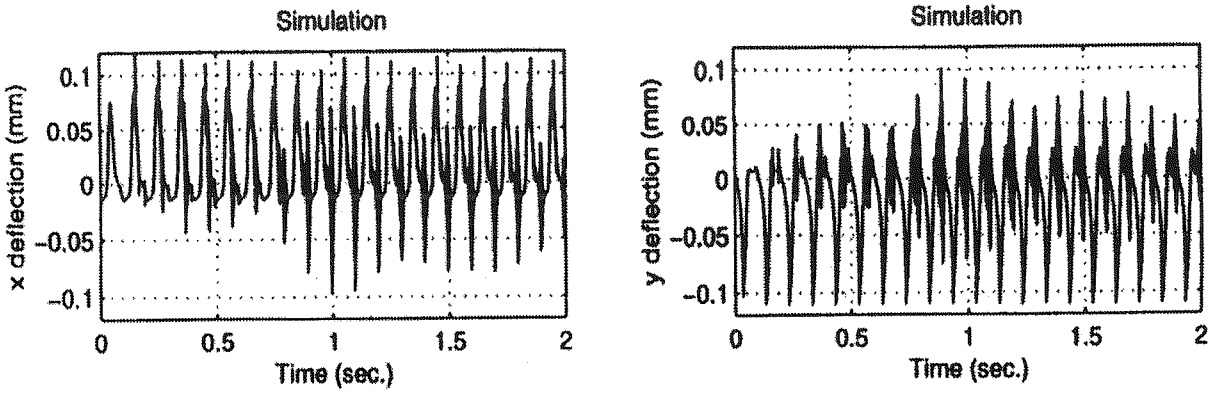

(a) Dynamic simulation and experimental force components

Figure (10) (a) Dynamic simulation and experimental force components for $\Phi = 15^{\circ}$, $\Psi = 0^{\circ}$
(b) Simulation of tool tip deflection in x and y directions

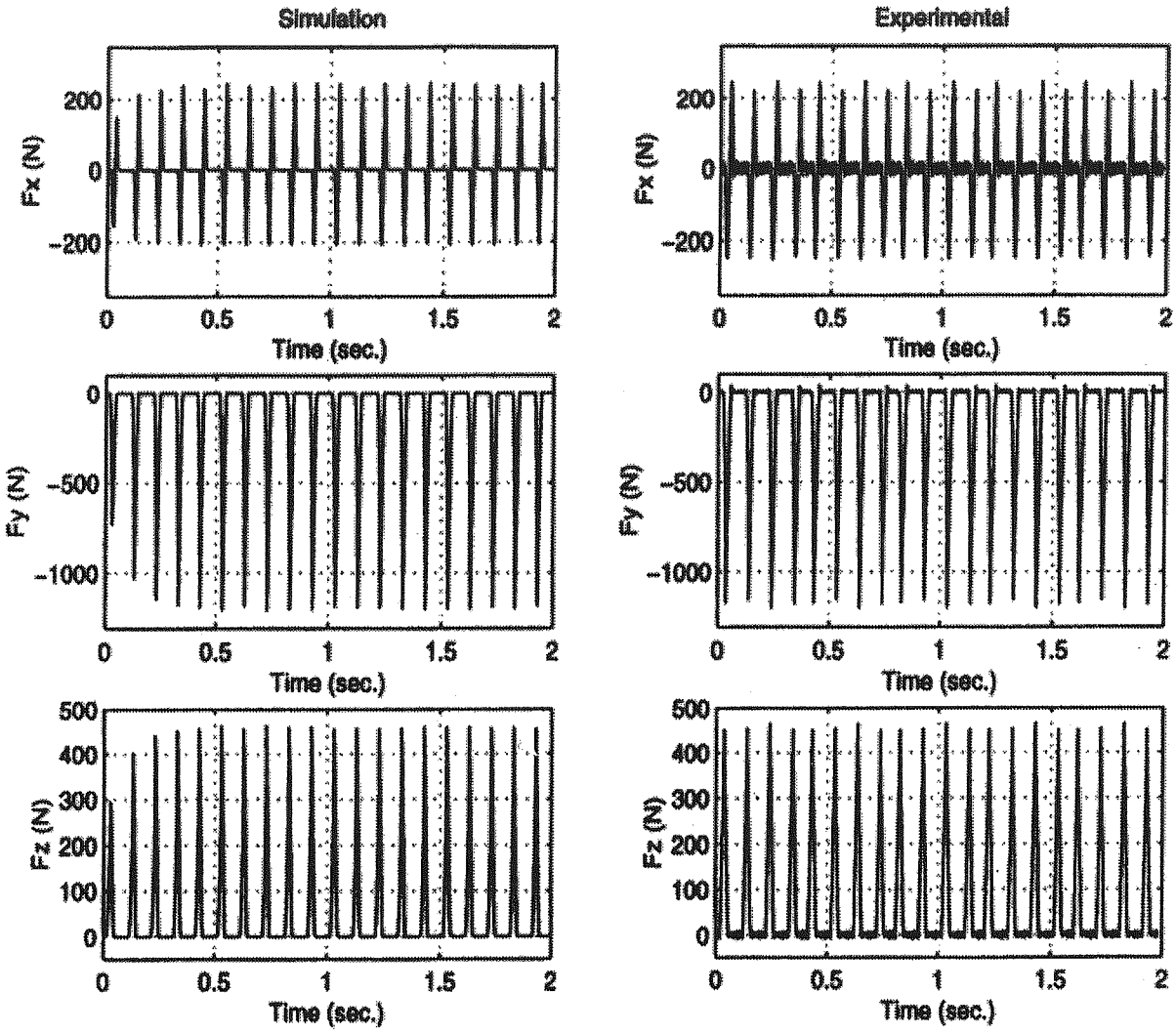

(a) Dynamic simulation and experimental force components

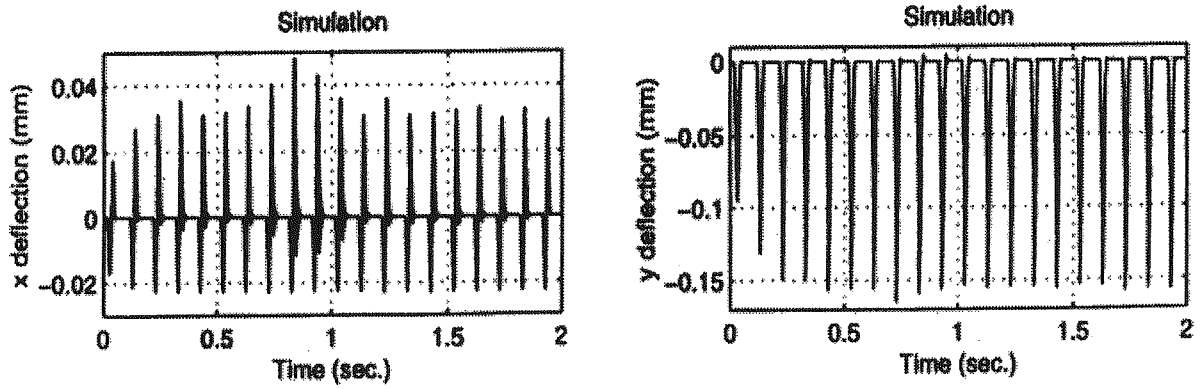

(b) Simulation of tool tip deflection in x and y directions

Figure (9)(a) Dynamic simulation and experimental force components for $\Phi = 15^{\circ}$, $\Psi = 0^{\circ}$
(b) Simulation of tool tip deflection in x and y directions.

forces and tool deflection can be predicted using the proposed model. The developed model allows process planners to generate appropriate cutting conditions in die ball-end milling .

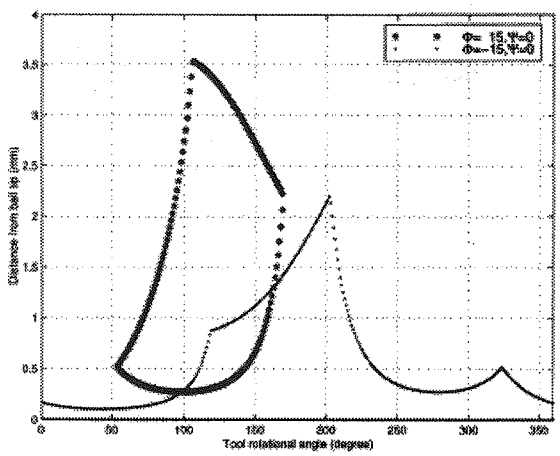

(Φ = - 15°,Ψ = 0°) and (Φ = 15°, Ψ= 0°)

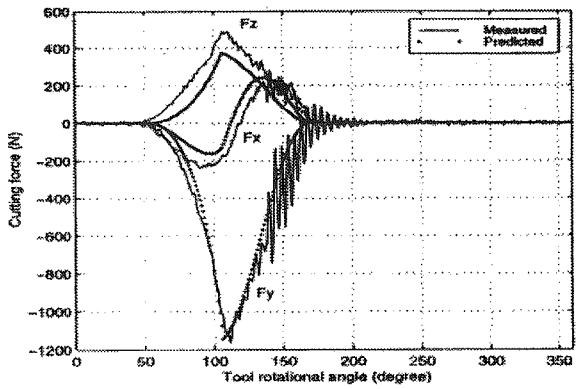

(static simulation) components for Φ = 15°,Ψ = 0°

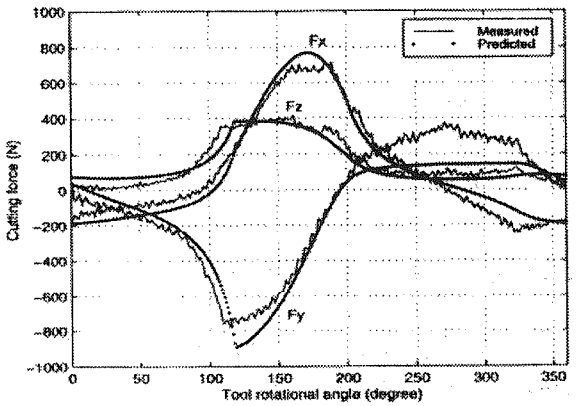

simulation) components for Φ=-15° , Ψ = 0°

Nomenclature

x, y, z	Cartesian coordinates
dz	differential length in axial direction
db	differential cutting edge length in the direction perpendicular to the cutting velocity
dF_{ct} , dF_{cr}, dF_{ca}	differential cutting forces in tangential , radial and axial directions
dF_{cx}, dF_{cy}, dF_{cz}	differential cutting forces in Cartesian coordinates
dF_{pt} , dF_{pr}	diferential ploughing forces in tangential and radial directions
dF_{px} , dF_{py}	diferential cutting forces in Cartesian coordinates
F_{cx} , F_{cy} , F_{cz}	total cutting forces in Cartesian coordinates
F_{px} , F_{py}	total ploughing forces in Cartesian coordinates
K_t, K_r, K_a	tangential , radial and axial cutting force coefficients
f_{sp}	specific ploughing force
f	feed per tooth
t(Θ ,z)	chip thickness at tool rotational angle of Θ and at axial location of z
R	ball radius
i(z)	helix angle at axial location of z
R(z)	ball radius in x-y plane and at axial location of z
r	a vector from reference point to a point on the cutting edge
η_c	chip flow angle
θ (z)	angle between ball tip (z=0) and a point on the cutting edge at axial location z
Θ	tool rotation angle about z axis

velocity of the differential element in the x-y plane and can be calculated by:

$$u = \dot{x} \sin \psi(\Theta, z) - \dot{y} \cos \psi(\Theta, z) \qquad (19)$$

where $\dot{x}$ and $\dot{y}$ are velocity of the tool tip in the x and y directions respectively.

The Cartesian components of the ploughing forces can be calculated using the following equations:

$$dF_{px} = -\sin \psi(\Theta, z)\, dF_{pr} - \cos \psi(\Theta, z)\, dF_{pt}$$

$$dF_{py} = \cos \psi(\Theta, z)\, dF_{pr} - \sin \psi(\Theta, z)\, dF_{pt} \qquad (20)$$

The total ploughing force components at tool rotation angle of Θ, in Cartesian coordinates, can be calculated by:

$$\{F_{px}, F_{py}\} = \int_{z_l}^{z_u} \{dF_{px}, dF_{py}\}\, dz \qquad (21)$$

5-Model verification

Ball-end milling experiments using $2\frac{1}{2}$ axis CNC milling maching were performed in order to verify the model simulation results. A 16 mm diameter, 20° rake angle, 9° clearance angle, one flute ball-end mill was used in the experiments. The workpiece material was steel AISI 1045. The ball-end milling experiments were performed in down milling mode and without coolant. The machining forces were measured using a three component force dynamometer, Kistler type 9255B. The spindle speed, depth of cut, and width of cut (Δy) were set to 600 rpm, 2 mm and 4 mm, respectively. The workpiece surface had two angles, one angle relative to x direction, Φ, and the other angle relative to y direction, Ψ, as shown in Fig. 2. Fig. 6 shows the integrations limits for two cases, one case with Φ= 15° and Ψ =0° (uphill machining) and the other case (downhill machining) with Φ= - 15° and Ψ = 0°. In the case of (Φ= 15°, Ψ = 0°), the cutting edge engagement span is from tool rotational angle of 54° to 169°. However for the case of (Φ= - 15°,Ψ=0°) the engagement span is from angle of 0° to 360°. The static cutting forces are shown in Fig. 7 and Fig. 8. The predicted and measured dynamic forces and the tool tip deflection are show in Fig. 9 and Fig. 10. It can be seen that the predictions are in reasonable agreement with the measured results.

6-Conclusion

This paper represents an approach for prediction of the static cutting forces, the dynamic forces and tool deflection in machining of die surfaces with ball-end mills. The are cutting edge and updated part geometry modeled using a commercially available geometric modeler (ACIS). The engaged portions of the cutting edge are extracted and used by force model. The cutting forces generated by each element on the portion of the engaged cutting edge, are evaluated by applying classical oblique cutting transformation on orthogonal cutting data. For calculation of ploughing forces, Wu's model is extended to the ball-end milling process. The total force components (including cutting forces and ploughing forces) for each tool rotation step are calculated by summing up the differential force components.

The die surface can be approximated by a set of elemental planar surfaces with two angles, one angle relative to x direction, Φ, and the other angle relative to y direction, Ψ.

Therefore for each tool location the Φ and Ψ angles can be calculated, and the dynamic

where κ is the angle in a vertical plane between a line from cutter center to a point on the cutting edge and z axis as shown in Fig. 4.

Finally, the cutting force components at tool rotation angle of Θ can be expressed as:

$$\{F_{cx} F_{cy} F_{cz}\} = \int_{Zl}^{z_u} \{dF_{cx}, dF_{cy}, dF_{cz}\} dz \qquad (15)$$

The integration limits, z_l and z_u are the engaged portion of the cutting edge with updated part at tool rotation angle of Θ. In order to compute the integration limits, a solid modeling based simulator of the ball-end milling process is developed. A commercially geometric solid modeler (ACIS) is used for representing the tool solid model, the cutting edge and the updated part. The updated part is constracted by performing a boolean subtraction operation between the part and the tool swept volume. The contact face between the ball-end mill and the updated part includes all the information to calculate the integration limits.

4-2-Ploughing force model

The ploughing forces acting on an element of the cutting edge due to indentation of the tool into the working material are given by Wu [12]:

$$dF_{pr} = f_{sp} dv$$

$$dF_{pt} = \mu_c dF_{pr} \qquad (16)$$

where dF_{pr} and dF_{pt} are the radial and tangential ploughing force components (see Fig. 5), μ_c is the mean friction coefficient between the flank and the workpiece, dv is the volume of work material displaced by the tool penetration, and f_{sp} is the specific ploughing force. For steel, the value of f_{sp} is 4.1×10^5 N/mm^3, and μ_c is 0.3 [12]. To compute dv, the engaged portion of the cutting edge is divided into a number of differential elements in the axial direction and each axial element analysed as an orthogonal process and the relations introduced in [12]

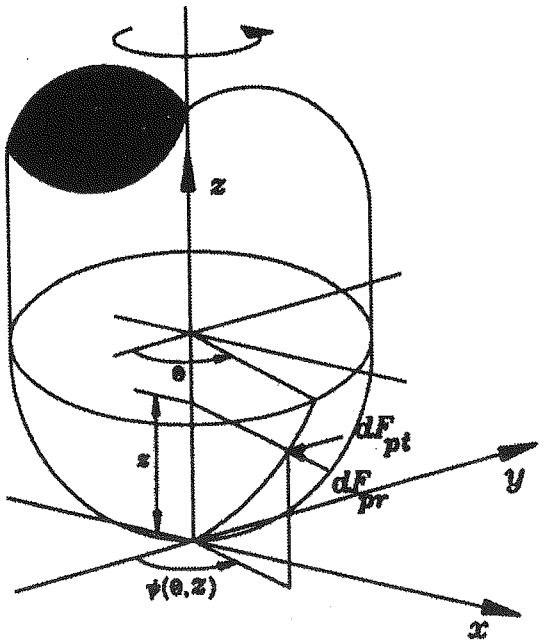

Figure (5) Elemental ploughing force components acting on the cutting edge.

for computing dv are used as follows:

$$dv = \left[\frac{V}{V \tan\gamma_0 + \dot{u}} - \frac{\tan\gamma_0}{2} \left(\frac{V}{V \tan\gamma_0 + \dot{u}} \right)^2 \right] \eta^2 dz \qquad (17)$$

$$\eta = 0.0046 + 0.005 \frac{t(\Theta, z)}{\sin\phi} \qquad (18)$$

where ϕ is the shear angle, V is the cutting speed, γ_o is the tool clearance angle, dz is the differential length in axial direction and $\dot{u}$ is

radial, dF_{cr}, and axial, dF_{ca} cutting forces acting on an element in tool rotational position of Θ and at axial location of z (see Fig. 4) are given by:

$$dF_{ct} = K_t t_n(\Theta, z)\, db$$

$$dF_{cr} = K_r t_n(\Theta, z)\, db$$

$$dF_{ca} = K_a t_n(\Theta, z)\, db \qquad (9)$$

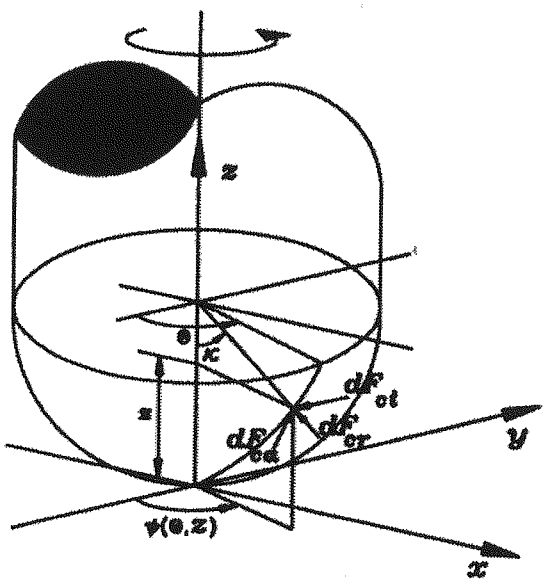

Figure (4) Elemental cutting force components acting on the cutting edge.

where $db = \frac{dz}{\cos k}$, $\kappa = \arcsin\frac{R(z)}{R}$, $t_n(\Theta, z) = t(\Theta, z)\sin k$. The cutting force coefficents K_t, K_r and K_a are identified from orthogonal data base according to the following oblique transformation [15]:

$$K_t = \frac{\tau}{\sin\phi_h}\,\frac{\cos(\beta_n - \alpha_n) + \tan\eta_c \sin\beta_n \tan i}{c}$$

$$K_r = \frac{\tau}{\sin\phi_n \cos i}\,\frac{\sin(\beta_n - \alpha_n)}{c}$$

$$K_a = \frac{\tau}{\sin\phi_h}\,\frac{\cos(\beta_n - \alpha_n) - \tan\eta_c \sin\beta_n}{c}$$

$$c = \sqrt{\cos^2(\beta_n - \alpha_n) + \tan^2\eta_c \sin^2\beta_n} \qquad (10)$$

The normal friction angle, β_n, and normal shear angle, ϕ_n, in oblique cutting are [15]:

$$\tan\beta_n = \tan\beta\cos\eta_c \qquad (11)$$

$$\tan(\phi_n + \beta_n) = \frac{\cos\alpha_n \tan i}{\tan\eta_c - \sin\alpha_n \tan i} \qquad (12)$$

where α_n is the normal rake angle and η_c is the chip flow angle. Stabler's chip flow rule $\eta_c = i$ is assumed [16].

The shear stress, τ, friction angle, β, and shear angle, ϕ, for steel AISI are modeled using the following equations [10]:

$$\tau = 1.586\,(vf)^{-0.25} + 67.703$$

$$\phi = 106.7(vf)^{0.5} + 0.375\alpha_e + 13.64$$

$$\beta = 48.4(vf)^{0.125} + \alpha_e - \phi + 28.586 \qquad (13)$$

where α_e, ϕ and β are in degree, τ in kgf/mm^3 and V is the cutting speed in m/min and α_e is the effective rake angle, The differential cuting forces calculated using equation (9) are transformed to Cartesian coordinates as follows:

$$dF_{cx} = -\sin k \sin\psi(\Theta, z)\, dF_{cr} - \cos\psi(\Theta, z)\, dF_{ct} + \cos k \sin\psi(\Theta, z)\, dF_{ar}$$

$$dF_{cy} = +\sin k \cos\psi(\Theta, z)\, dF_{cr} - \sin\psi(\Theta, z)\, dF_{ct} - \cos k \cos\psi(\Theta, z)\, dF_{ar}$$

$$dF_{cz} = \cos k\, dF_{cr} + \sin k\, dF_{ar} \qquad (14)$$

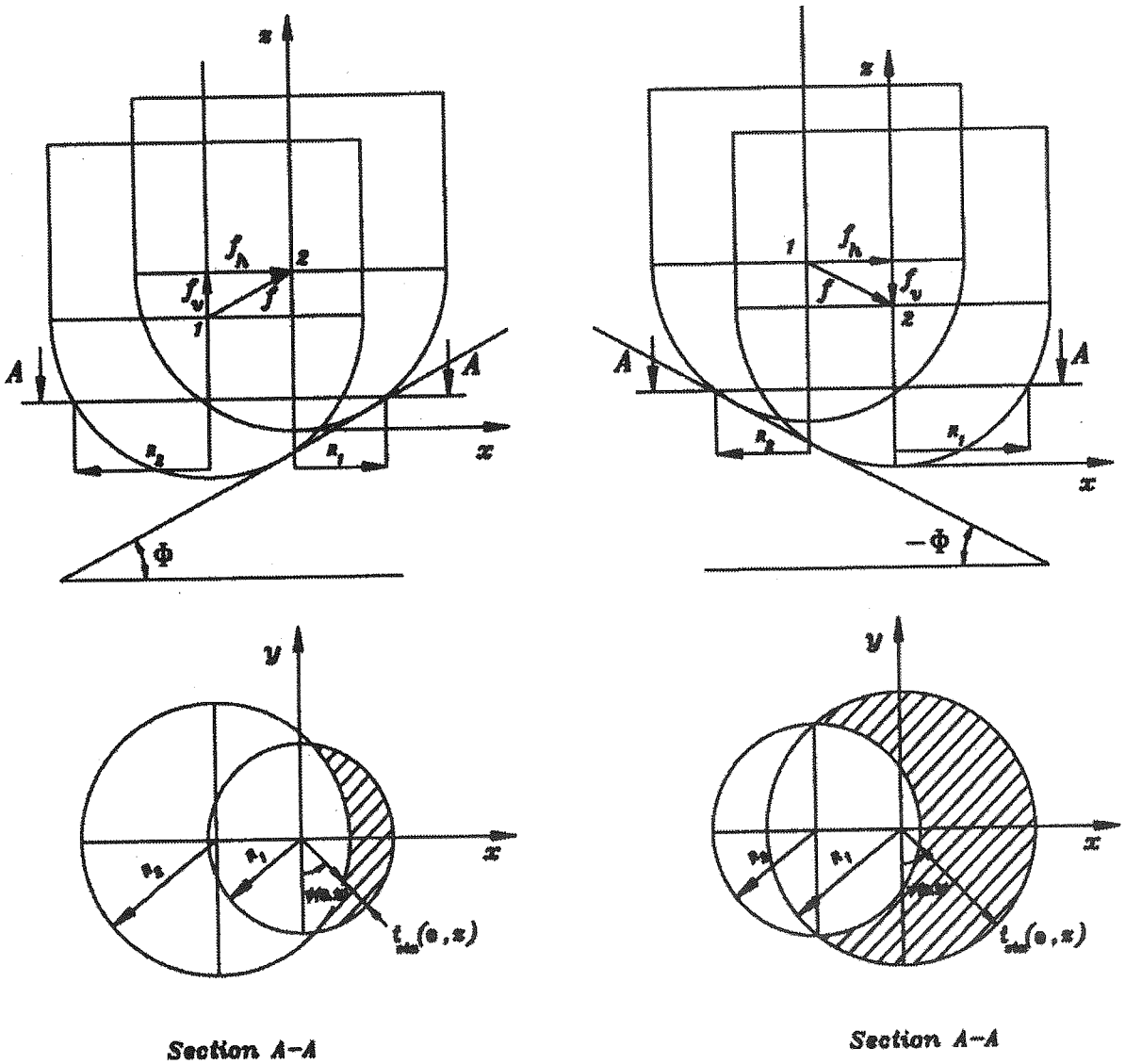

(3-a) $\Phi > 0$ (3-b) $\Phi < 0$

Figure (3) Chip thickness in 3-axis ball - end milling process.

static chip thickness can be expressed as follows:

$$t_{sta}(\Theta, z) = \frac{R-z}{\sqrt{R^2 - (R-z)^2}} f_v + f_h \sin\psi(\Theta, z) \quad (8)$$

where $f_v = f \sin\phi$, $f_h = f \cos\phi$.

In the case of 3-axis ball-end milling with $\phi<0$ (see Fig . 3-b) , sign of f_v is negative and the chip thickness can be calculated from Eq. 8. when $\phi = 0$, $R_1(z)$ and $R_2(z)$ are equal and $t_{sta}(\Theta, z) = f_h \sin\psi(\Theta, z)$.

4-Force prediction

4-1-Cutting force model

For the calculation of cutting forces, the unified approach introduced by Budak et al . [15] is extended to the ball-end miling process. The elemental tangential, dF_{ct} ,

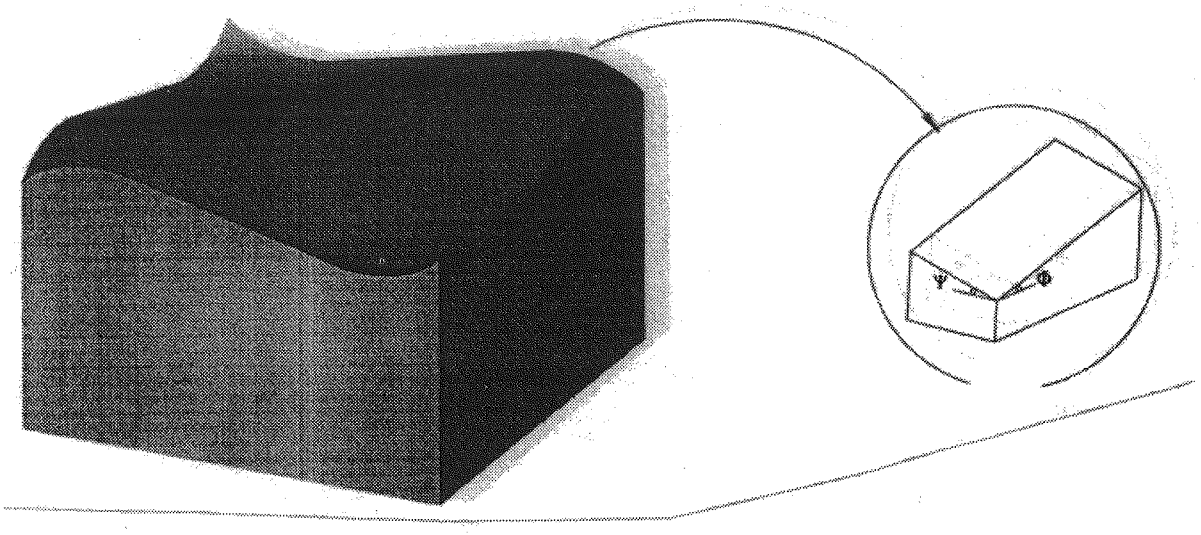

Figure (1) Die Surface and an element of it.

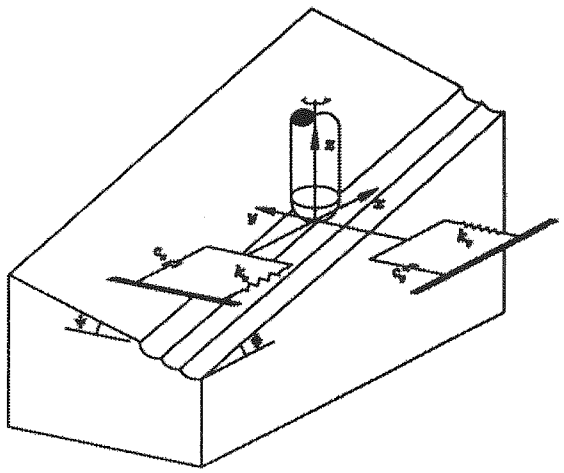

Figure (2) The vibratory model of the ball-end mill.

where $t_{sta}(\Theta, z)$ is the static chip thickness at tool rotational angle of Θ and at axial location of z, x and y are deflections of the tool tip at the present time, u_{-1} is the undulation that could be left from the previous tooth and it can be expressed as:

$$u_{-1} = x_{-1} \sin\psi(\Theta, z) - y_{-1} \cos\psi(\Theta, z) \quad (5)$$

where x_{-1} and y_{-1} are tool tip deflections at the previous time, $\psi(\Theta,z)$ is the rotational position of a point on the cutting edge at tool rotational angle of Θ and axial rotation of z. For calculation of the static chip thickness in the case of 3-axis ball-end milling with $\Theta > 0$ (see Fig. 3-a), Lim. et al. [14] considered the effect of vertical component of the feed on the static chip thickness using the following relation:

$$t_{sta}(\Theta, z) = R_2(z) - R_1(z) + f_h \sin\psi(\Theta, z) \quad (6)$$

where f_h is the horizontal component of the feed, $R_2(z)$ and $R_1(z)$ are the ball-nose radii at two successive positions at the same z value (see Fig. 3). The difference between $R_2(z)$ and $R_1(z)$ is due to the vertical height difference of f_v. Therefore this difference can be approximated by:

$$R_2(z) - R_1(z) \simeq \frac{dR(z)}{dz} f_v \quad (7)$$

where $R(z) = \sqrt{R^2 - (R - z)^2}$ and $\frac{dR(z)}{dz} = \frac{R-z}{\sqrt{R^2-(R-z)^2}}$.

with combining the above equations the

coefficient, structural transfer functions and the geometry of the ball-end mill. These models were applicable to ball-end milling of horizontal planar surfaces only.

The aim of the present investigation is to develop a dynamic force model for fast evaluation of ball-end milling forces and tool deflections in different locations of a die surface. A commercially available solid modeler, ACIS [11], is used to represent the cutting edge, tool and updated part geometries. The cutter-part engagment is computed using the contact face between the ball-end mill and the updated part. The instantaneous chip thickness is computed by summing up the static chip thickness, the tool deflection and the undulations left from the previous tooth. The geometric information and the cutting parameters are used in an orthogonal cutting data base of the ball-end milling process to determine the dynamic forces. In order to include the effect of the interference of the tool flank face with the finished surface of the work, the ploughing force model introduced by Wu [12] is extended to the ball-end milling process. The total forces (including the cutting and ploughing forces) are applied to the structural vibratory model of the system and the dynamic deflections at the tool tip are predicted. The model is verified at different cutting conditions.

2-Vibratory model

A sculptured surface (e.g die surface) can be approximated by a set of elemental planar surfaces with two angles,Φ andΨ(see Fig. 1).

The vibratory model used in the simulation of milling operations has been described in several works (e.g. Tlusty and Ismail[13]). Fig. 2 shows a two-degree-of-freedom vibratory system in x and y directions for machining of a planar surface. This surface has two angles, one angle relative to x direction ,Φ , and the other angle relative to y direction, Ψ. Based on this coordinate system,the equilibrium equations of the vibratory model can be represented by:

$$m_x \ddot{x} + c_x \dot{x} + k_x x = F_{cx} + F_{px} \quad (1)$$

$$m_y \ddot{y} + c_y \dot{y} + k_y y = F_{cy} + F_{py} \quad (2)$$

where m_x, c_x, k_x are the structural parameters in the x direction, and m_y, c_y, k_y are the structural parameters in the y direction , respectively and F_{cx}, F_{cy} are the cutting forces in the x and y directions and F_{cy}, F_{py} are the ploughing forces in the x and y directions relatively. The differential equations (1) and (2) are solved using a fourth order Runge-Kutta scheme numerically at small time steps, Δt, which is selected ten times smaller than the period of the highest natural model in the simulation system[5]. The parameters used to define the vibratory system were obtained from modal testing and [13]:

$$m_x = m_y = 0.11 kg$$

$$\xi_x = \xi_y = 0.019,$$

(ξ is the damping ratio and $\xi = \frac{c}{2\sqrt{km}}$)

$$k_x = 8.1 \times 10^6 \text{ N/m}, \; k_y = 7.7 \times 10^6 \text{ N/m} \quad (3)$$

3-Instantaneous chip thickness

The instantaneous chip thickness can be obtained by[2]:

$$t(\Theta, z) = t_{sta}(\Theta, z) + [x \sin\psi(\Theta, z) - y\cos\psi(\Theta, z)] - u_{-1} \quad (4)$$

On the prediction of Cutting Dynamics in Ball-End Milling of Die Surfaces

H. Haghighat
PhD. graduate
Department of Mechanical Engineering
Tarbiat Modarres University

M. H. Sadeghi
Associate professor
Department of Mechanical Engineering
Tarbiat Modarres University

M. A. Elbestawi
Professor
Department of Mechanical Engineering
McMaster University

Abstract

An approach for dynamic simulation of ball-end milling of die surfaces is presented in this paper. It has the capability of estimating the static and dynamic cutting forces and tool deflections for various cutting conditions.A commercially available geometric engine is used to represent the cutting edge, cutter and updated part. The contact face between cutter and updated part is determined from the solid model of the updated part and cutter location. To determine cutting edge engagement for each tool rotational step, the intersections between the cutting edge with boundary of the contact face are determined. The instantaneous chip thickness is computed by summing up the static chip thickness, the tool deflection and the undulations left from the previous tooth. The geometric information and the cutting parameters are used in an orthogonal cutting data base of the ball-end miling process, from which the dynamic forces are obtained. For calculating the ploughing forces, Wu's model is extended to the ball-end miling process. The total forces, including the cutting and ploughing forces are applied to the structural vibratory model of the system and the dynamic deflections at the tool tip are predicted.The developed model is verified through experiments performed for several workpiece geometries and different cutting conditions.

1- Introduction

The ball-end milling process is widely used for machining of die surfaces. Research work has been reported in the literature related to dynamic simulation in flat end mills [1,2,3,4,5,6,7]. Unlike flat end mills, ball - end mill cutters have a variable radius, helix and rake angles along the cutting edge. Due to decreasing radius, the cutting speed reduces along the cutting edge, starting with the same value as the cylindrical portion and reaching zero at the tool tip. Studies for dynamic simulation of ball-end milling process have been reported by Abrari and Elbestawi [8] and Lee and Altintas [9]. Abrari and Elbestawi extended the concept of the equivalent orthogonal cutting conditions , applied to modeling of the mechanics of ball -end milling by Yang and park [10] , to include the dynamics of cutting forces. Lee and Altintas simulated ball-end milling process in time domain by considering the instantaneous regenerative chip load, local cutting force